Uncertainty in United States Coastal Wetland Greenhouse Gas Inventorying: Supplemental Information

James R Holmquist [1*] (HolmquistJ@si.edu)

Lisamarie Windham-Myers [2] (lwindham-myers@usgs.gov), Blanca Bernal [3,1] (BernalB@si.edu), Kristin B. Byrd [4] (kbyrd@usgs.gov), Steve Crooks [5] (steve.crooks.bc@gmail.com), Meagan Eagle Gonneea [6] (mgonneea@usgs.gov), Nate Herold [7] (nate.herold@noaa.gov), Sara H. Knox [8] (saraknox@stanford.edu), Kevin D. Kroeger [6] (kkroeger@usgs.gov), John McCombs [9] (John.McCombs@noaa.gov), J. Patrick Megonigal [1] (MegonigalP@si.edu), Lu Meng [1] (LuM@si.edu), James T Morris [10] (morris@inlet.geol.sc.edu), Ariana E. Sutton-Grier [11] (a.sutton-grier@tnc.org), Tiffany G. Troxler [12] (troxlert@fiu.edu), Donald E Weller [1] (WellerD@si.edu)

* Corresponding Author
1. Smithsonian Environmental Research Center, 647 Contees Wharf Rd, Edgewater, MD 21037, USA
2. National Research Program, U.S. Geological Survey, 345 Middlefield Road, Menlo Park, CA 94025, USA
3. Winrock International, 2121 Crystal Drive, Arlington, VA 22202, USA
4. Western Geographic Science Center, U.S. Geological Survey, 345 Middlefield Road, Menlo Park, CA 94025, USA
5. Silvestrum Climate Associates, 150 Seminary Drive, Mill Valley, CA 94941, USA
6. U.S. Geological Survey Woods Hole Coastal & Marine Science Center, 384 Woods Hole Rd., Woods Hole, MA 02543, USA
7. NOAA Office for Coastal Management, 2234 South Hobson Ave., Charleston, SC 29405-2413, USA
8. Department of Earth System Science, Stanford University, Stanford, CA 94305, USA
9. The Baldwin Group at NOAA Office for Coastal Management, 2234 South Hobson Ave., Charleston, SC 29405-2413
10. Belle Baruch Institute, University of South Carolina, Columbia, SC 29208, USA
11. Earth System Science Interdisciplinary Center, University of Maryland, College Park, MD 20740 and The Nature Conservancy, Bethesda, MD 20814, USA
12. Sea Level SOlutions CEnter and Southeast Environmental Research Center, Institute of Water and Environment, Florida International University, Miami, Fl, 33139, USA

1. Supplemental Information

Under the United Nations Framework Convention on Climate Change (UNFCCC), all Parties (countries) have agreed to report anthropogenic emissions by sources and removals by sinks, including from the land use, land-use change and forestry sector. Reporting is accomplished through the submission of national reports (National Communications and National GHG Inventories, biennial reports or biennial update reports), with different requirements for Annex I and non-Annex I countries (Iversen *et al* 2014). The United States EPA prepares the official U.S. Inventory of Greenhouse Gas Emissions and Sinks to comply with existing commitments under the UNFCCC.

In 2014, the IPCC released the 2013 Supplement to the 2006 IPCC Guidelines for National Greenhouse Gas Inventories: Wetlands (IPCC 2014). The Wetlands Supplement "extends the content of the 2006 IPCC Guidelines by filling gaps in coverage and providing updated information reflecting scientific advances, including updating emission factors for human activities on wetlands".

Chapter 4 of the Wetlands Supplement provides guidance on estimating emission and removals of greenhouse gases (CO_2, CH_4 and N_2O) associated with specific activities on managed coastal wetlands, which may or may not result in a land use change (Wetlands Supplement, Overview Chapter, p. O-8) (IPCC 2014). Regardless of whether a land-use change occurs or not, it is *good practice* to quantify and report significant emissions and removals resulting from management activities on coastal wetlands in line with their country-specific definition (IPCC 2014).

The Wetlands Supplement provides methodological guidance on managed coastal wetlands so that countries can, at a minimum, produce Tier 1 estimates of GHG emissions and removals for specific management activities that had been shown at the time of writing to be among the most significant anthropogenic activities in coastal wetlands globally (IPCC 2014). As it is known that a country's national circumstances will determine what anthropogenic activities are significant at a national scale, and that countries will have different levels of resources and data to report on their GHG emissions and removals, the emphasis of the Wetlands Supplement and the guidelines that precede it, is on enabling countries to meet the conditions set by their national circumstances and good practice in national GHG inventory compilation.

In this supplement we present additional details, methods, assumptions and references used to calculate our version of a contiguous united states (CONUS) coastal national greenhouse gas inventory (NGGI). We additionally discuss datasets that contributed less compared than others to overall uncertainty in greater detail. We provide interesting results, observations, and discussion regarding results of the analyses that were not discussed in the main text.

2. Additional Materials and Methods

Activities data were generating using the coastal change analysis program from 2006 to 2011, with additional interpretation of palustrine wetland categories done using digital elevation models (DEMs). A full accounting of spatial products download and utilized is available in supplemental table 1.

2.1. Probabilistic Mean Higher High Water Spring Maps

To create a probabilistic coastal lands map we utilized digital elevation models archived and aggregated by the NOAA sea-level rise viewer (NOAA 2016) (Supplemental Table 1). Some data sources for the San Joaquin Delta (Wang and Ateljevich 2012), Maryland State (Eastern Shore Regional GIS Cooperative n.d.), and the Northern Gulf of Mexico Region (USGS 2014) were not archived through the NOAA portal, so we cite the original data sources (Supplemental Table 1). All DEMs were relative the the NAVD88 datum. In the rare cases in which units were not in meters (m) relative to NAVD88, they were converted to m in ArcGIS Pro (Esri Inc. 2017).

For the LiDAR maps we corrected for bias and propagated random error by calculating mean error and root mean square error (RMSE) from weighted averages from a literature review (Hladik *et al* 2013, Medeiros *et al* 2015, Buffington *et al* 2016, Holmquist *et al* in Prep) (Supplemental Table 3). If a LiDAR pixel intersected a wetland as mapped by C-CAP data (NOAA 2013) we applied an average 17.3 cm offset using ArcGIS (Esri Inc. 2017) (Supplemental Fig. 1).

To transform the NAVD88 datum of the LiDAR DEMs to a tidal datum, we used NOAA tide gauge data. For the NAVD88 to MHHW datum transformation, we used NOAA datums which had established MHHW and a NAVD88 datum (NOAA 2017). To establish datum uncertainty we used NOAA's reported standard errors for tidal datum transformation (NOAA n.d., n.d., n.d.). This included 705 gauges. To transform MHHW to MHHWS we calculated MHHWS offsets at gauges using NOAA high-low tide data (NOAA CO-OPS n.d.) and astronomical records of full and new moons (USNO n.d.). We assumed that the spring tides occur twice monthly and can have occur between one day before to two days after a full or new moon. We queried NOAA servers for all of those gauges over the most recent datum period for the gauge and represented MHHWS relative to MHHW as the mean offset over those time periods. We represented uncertainty in the datum itself by estimating the standard error of the mean (Eq. 1). There was a notable and precipitous increase in standard error for gauges that had few observations of spring tides, which we detected using a piecewise linear regression (Sonderegger 2012). So we excluded tide gauges from the analysis that had fewer than 31 datapoints. 127 tide gauges were included in the MHHW to MHHWS transformation.

$$se = \frac{sd}{\sqrt{n}} \qquad 1.$$

In which:

se = standard error of the mean

sd = standard deviation

n = sample size

For the NAVD88 to MHHW transformation and MHHWS to MHHW offset we extrapolated point data to a 2-d surface using Empirical Bayesian Kriging (EBK) (Pilz and Spöck 2008, Krivoruchko 2012). We reduced the resolution of both datum transformation layers 300 x 300 m, with pixel edges snapped to C-CAP's dimensions.

Our goal in creating a probabilistic MHHWS layer was to reflect uncertainty in both the datums themselves (areas with lower-quality datums have greater uncertainty than areas with higher-quality datums), as well as distance from gauges (areas further away from any gauge have greater uncertainty than those nearer). We calculated total propagated error for NAVD88 measurement, MHHW transformation and MHHWS transformation. For the NAVD88 surface we used the weighted mean RMSE for wetland surfaces from multiple studies (Supplemental Table 2). For tidal datum transformations we incorporated for two types of uncertainty: 1. uncertainty in the extrapolation process itself -- the standard error of prediction from the empirical bayesian kriging output -- and 2. uncertainty in the datums themselves (NOAA n.d., n.d., n.d.), also extrapolated from points to a 2-d surfaces using empirical bayesian kriging. EBKs were run in ArcGIS pro (Esri Inc. 2017) with a power semivariogram model, 100 maximum points for each local model, a local model area overlap factor of 1, 100 simulated semivariograms, a standard circular neighborhood with a radius of 15, and max and min neighbors of 15 and 10 respectively.

We calculated total propagated uncertainty in all of the transformations algebraically (Eq. 2). We resampled raster resolutions of the DEMs to 30 x 30 m to match C-CAP. At the pixel level we calculated a Z-score according to Eq. 3 (Schmid *et al* 2013). We used the function ‘z2p’ in Python’s (Continuum Analytics, Inc 2017) NumPy package (NumPy Developers 2017) to calculate a ‘p value’ -- probability of a pixel being below MHHWS -- from the standard score.

$$se_{total(x,y)} = \sqrt{RMSE_{LiDAR}^2 + se_{MHHW(x,y)}^2 + se_{krig.1(x,y)}^2 + se_{MHHWS(x,y)}^2 + se_{krig.2\,(x,y)}^2} \qquad 2.$$

In which:

$se_{total(x,y)}$ = the total propagated uncertainty of the transformation for point x,y
$RMSE_{LiDAR}$ = the root-mean square error for LiDAR-based DEMs for marsh surfaces
se_{MHHW} and se_{MHHWS} = the standard errors of the datums at point x,y
$se_{krig.1}$ and $se_{krig.2}$ = the standard error of prediction resulting from the EBK process for MHHW and MHHWS respectively at point x,y

$$Z_{(x,y)} = \frac{(water\ surface_{(x,y)} - elevation_{(x,y)})}{se_{total\,(x,y)}} \qquad 3.$$

In which:

$Z_{(x,y)}$ = the standard score of point x,y
Water $surface_{(x,y)}$ = elevation of MHHWS relative to NAVD88 at point (x,y)
$elevation_{(x,y)}$ = elevation of the surface at point (x,y) relative to NAVD88

The number of palustrine stable and change 2006 to 2011 category, excluding changes to and from estuarine wetlands, totaled to 111. For each of these categories we extracted values from the probabilistic inundation map using ‘extract by mask’ in ArcGIS Pro (Esri Inc. 2017). The results were saved in separate tables and probabilities were rounded to a precision of 4 decimal points.

We downloaded and mosaiced C-CAP data from all coastal states (both oceanic and Great Lakes) (NOAA 2013). As a first step we extracted mapped areas for palustrine and estuarine stable wetland and 2006 to 2011 wetland changes. For each of 111 palustrine stable and change classes we approximated mapped area as a normal distribution using Eq. 4 and 5 .

$$\mu = \sum_{i=1}^{N} n\phi_i \quad 4.$$

In which:

mu = mean of the normal approximation

N = number of probability classes

i = is a probability class in n probability classes

n = the number of pixels in probability class i

phi = the probability of class i

$$\sigma^2 = \sum_{i=1}^{N} n\phi_i(1-\phi_i)\, 5.$$

In which:

sigma squared = variance of the normal approximation

The probabilistic model for palustrine mapped area assumes complete independence of error at the pixel level, however remaining error is likely correlated based on the source of the DEM, the individual LiDAR surveys, or event the passes within a LiDAR survey. Modeling correlation of errors at the pixel level may require re-analysing the original LiDAR point-cloud data, which is beyond the scope and computational constraints of this exercise.

2.2. C-CAP Accuracy Assessment

For the remaining 129 estuarine stable and 2006 to 2011 change classes, we represented mapped area as is in C-CAP and treated them as fixed values (Supplemental Fig. 1). To estimate area and incorporate uncertainty in C-CAP classification and change detection, we utilized C-CAP's 2011 23 class accuracy assessment, C-CAP's 2006 to 2011 accuracy assessment for change and no-change, and C-CAP 2006-2010 area data from all coastal states (both ocean and Great Lakes). We calculated proportional area accuracy assessment matrix (Eq. 6) and calculated estimated area (Eq. 7) (Olofsson *et al* 2014).

$$\hat{p}_{i,j} = W_i \frac{n_{i,j}}{n_i} \quad 6.$$

In which:

$p_{i,j}$ = the proportional area of reference class j mapped as class i

W_i = proportion of mapped area for class i

$n_{i,j}$ = sample counts for reference class j mapped as class i

$n_{i.}$ = sample counts for mapped class i

$$\hat{p}_{.j} = \sum_{i=1}^{q} \hat{p}_{i,j}\, 7.$$

In which: $p.hat_{.j}$ = the estimated proportional area of reference class j

$$r_j = \frac{estimated.area_j}{mapped.area_{i=j}} \quad 8.$$

In which: r_j is the ratio of estimated to mapped landcover j

With equation 6 we transformed the accuracy assessment matrix from counts to proportional areas. In equation 7 we calculate an estimated area as the column sum of a class in the proportional area confusion matrix. We calculated an estimated area for the entire C-CAP extent and represented it as a scaler *r*, the ratio of estimated to mapped area for smaller subsections of the map (Eq. 8).

We could have represented estimated area uncertainty in the Monte Carlo analysis as a normal distribution following the best practices for estimating standard error of the estimate (Olofsson *et al* 2014, Byrd *et al* 2018). However, this would make the assumption that errors were symmetrical; some key classes were skewed towards over or under-mapping. So, we decided to represent the accuracy assessment data itself as a 23 separate probability distributions, simulate the accuracy assessment as a random draw from those distributions for each iteration of the Monte Carlo analysis, and recalculate estimate to mapped area ratios. We modeled each reference class as a multinomial distribution with 23 possible mapped classes. We did the same for 2006 to 2011 change and no change analysis.

For each iteration of the Monte Carlo analysis we scaled mapped estuarine area (which was fixed) and mapped palustrine area (which was a random draw from a normal distribution) separately by the estimated to mapped area ratio for the 2011 class and for either 2006 to 2011 change or no change.

In the Monte Carlo Analysis we redrew the accuracy assessment data using the multinomial distribution. The multinomial distribution could be described by two parameters, the total number of observations for the mapped class i (η_i) and a vector of probabilities, each instance indicating the probability of the reference class being mapped as a category (ϕ_i). For each row in an accuracy assessment matrix η_i is equal to the column sum and is ϕ_i a vector for reference class i containing each reference value (column value) divided by η_i (row sum) (Eq. 9).

$$A_i \sim multinom(\eta_i, \boldsymbol{\phi_i}) \qquad 9.$$

In which: A is a square accuracy assessment matrix and A_i is a row i representing mapped class i

2.3. Emissions Factors

For all emissions and storage factors reported in units relative to organic carbon mass, we converted to CO_2-equivalents using a conversion factor of 3.667 $gCO_2\ gC^{-1}$. We made other area and mass conversions throughout to convert units as reported all emissions factors in their original text to $gCO_2\ m^{-2}\ yr^{-1}$. These included converting hectares to m^2 (10,000 $m^2\ ha^{-1}$), C-CAP pixels to m^2 (900 $m^2\ pixel^{-1}$), Pg to g (1E15 $g\ Pg^{-1}$), and kg to g (1,000 $g\ kg^{-1}$). Final reports of emissions summed at the national scale were made in millions of metric tonnes of CO_2e per year (yr^{-1}).

2.3.1. Soil Fluxes

If wetlands remained wetlands, we assumed carbon burial occurred annually over the full five years. If wetland area were gained from another category, or were lost to other categories but soil mass was not lost, we assumed carbon was buried over half that time, 2.5 years. We assumed changes from wetlands to open water and unconsolidated shore, estuarine and palustrine aquatic beds, cultivated and pasture/hay, or developed (high, medium, and low intensity) land cover classes represented soil loss events, while other conversions such as to grasslands, forests, or bare land, did not.

We used a review of carbon accumulation rates (CAR) from a literature review created for the next iteration of the U.S. NGGI (Lu *et al* 2017). The CAR data selected for this compilation was obtained from published peer-reviewed manuscripts and reports that specifically presented single CARs associated to a coring location; manuscripts reporting CAR ranges or total averages from multiple coring locations were excluded. The type of data taken from these publications was either in the form of an actual CAR, or calculated from the reported soil accretion rate and (1) organic soil carbon pool, or (2) organic soil carbon content and soil bulk density. This database only contains long-term soil accretion or soil C accretion data, determined with ^{137}Cs, ^{210}Pb, pollen, or ^{14}C. Publications with rates estimated with eddy covariance, or short-term accretion rates such as horizon markers were not included. In this paper we used a subset of the data presenting ^{210}Pb-based records. Citations used herein follow: (Lynch 1989, Kearney and Stevenson 1991, Roman *et al* 1997, Orson *et al* 1998, Craft and Richardson 1998, Merrill 1999, Hussein *et al* 2004, Church *et al* 2006, Callaway *et al* 2012a, 2012b, Bianchi *et al* 2013, Crooks *et al* 2014, Weston *et al* 2014, Villa and Mitsch 2015, Marchio *et al* 2016, Noe *et al* 2016).

For soil carbon stock change associated with wetland loss, we used average soil carbon density values (mean = 0.027 gC cm^{-3} , s.d. = 0.013, n = 8280 samples) (Holmquist *et al* 2018) to characterize the CO_2 emission rate.

2.3.2. Biomass Fluxes

For flux related to biomass change we used multiple datasets. For emergent and scrub/shrub we used the calibration and validation data produced and compiled as part of a national remotes sensing dataset (Byrd *et al* 2018). Of 2,400 plots reported in the dataset, almost all were dominated by emergent vegetation, though 8 plots had 50% or greater cover of the shrub *Iva frutescens*, which we assumed qualified them as dominated by scrub/shrub according to C-CAP classifications (NOAA Office of Coastal Management n.d.).

To generate national scale metrics of mean flux associated with changes to or from forested wetland, and to further supplement the scrub/shrub data from Byrd et al. (2018), we performed a cursory database search and literature data synthesis. We archived tree diameter at breast height (DBH) measurements and plot areas for six studies (Megonigal *et al* 1997, Simard *et al* 2006, Doughty *et al* 2016, Craft *et al* 2017, Krauss *et al* 2018, Twilley *et al* 2018). We estimated above ground biomass (AGB) per unit area estimated at the level of the plot as the fundamental unit of inclusion in this synthesis.

For tidal freshwater forested wetlands we converted DBH to AGB using the following allometric equations. For (Megonigal *et al* 1997) we used allometric equations listed within. We note one correction to appendix 2; *Fraxinus* spp. DBH values need to be converted from centimeters to inches before input into the function, mass needs to be converted pounds to kilograms after output. For (Krauss *et al* 2018) and (Craft *et al* 2017) we utilized generic genus-specific allometric equations listed in (Jenkins *et al* 2003).

For mangroves we used to following allometric equations. For (Simard *et al* 2006) and (Doughty *et al* 2016) we used allometric equations listed therein. For (Twilley *et al* 2018) we used allometric equations originating from (Smith and Whelan 2006).

For each plot we summed biomass and divided total biomass by plot area to calculate AGB in grams per m^2. However (Simard *et al* 2006), used a variable area plot methodology. For these plots we followed the authors methodology calculating tree area to plot area ratio for each sampling area by multiplying the basal area factor of the prism they used to determine tree inclusion (BAF; 5 tree area [m^2] plot area [ha^{-1}]) by the number of trees within the plot. For each tree we calculated plot area from each tree area. For each tree we calculated biomass per hectare, and for each sampling area we calculated the average biomass per plot area. We also synthesized tree height data when available, to classify plots as shrub/scrub if average tree height was below 5 m and forested if above (NOAA Office of Coastal Management n.d.).

For studies that measured the same plots multiple times, we averaged the total plot biomass over all the sampling instances. We did not include belowground biomass, because the vast majority of studies referenced by (Holmquist *et al* 2018) made no note of removing root material from soils, so we assumed that root matter was part of the soil profile. We converted all AGB biomass values to carbon using a single conversion factor (Byrd *et al* 2018). We realize that this is an oversimplification for forested biomass data. However we intend this to be a first cut used for the purposes of uncertainty and sensitivity analysis, not to make definitive or authoritative statements about the carbon properties of various communities and species of forested wetland trees.

2.3.3. Methane Fluxes

In total, CH_4 flux measurements were available at 51 sites in North America (Windham-Myers and Cai in Revision). While chambers were used to estimate annual CH_4 fluxes at the majority of the sites, fluxes at two of the sites were measured using the using the eddy covariance method. Sources used in this analysis follow: (DeLaune *et al* 1983, Bartlett *et al* 1985, 1987, Kelley *et al* 1995, Magenheimer *et al* 1996, Neubauer *et al* 2000, Megonigal *et al* 2002, Marsh *et al* 2005, Poffenbarger *et al* 2011, Krauss and Whitbeck 2012, Neubauer 2013, Reid *et al* 2013, Segarra *et al* 2013, Weston *et al* 2014, Wilson *et al* 2015, Chmura *et al* 2016, Holm *et al* 2016, Krauss *et al* 2016, Mueller *et al* 2016).

2.3.4. Additional Detail on Monte Carlo Analysis

We simulated the central tendency of each input variable 10,000 times in R (R Core Team 2017) using random draw functions for the appropriate probability distributions (runif, rnorm, rlnorm, rmultinom). We required a separate R package for truncated normal distributions; we generated simulated datasets using the ‘rtruncnorm’ function in the ‘truncnorm’ package in R (Mersmann *et al* 2018). Running the analysis on a single core took a prohibitively long time using a single core, so we parallelized the execution of the Monte Carlo uncertainty analysis using the R Packages ‘foreach’ (Microsoft and Weston 2017), ‘doParallel’ (Revolution Analytics and Weston 2015), and ‘doSnow’ (Microsoft Corporation and Weston 2017).

For burial and storage data we performed the the same number random draws as the input dataset size, and represented the emissions factor using the central tendency (mean or logmean) as the defined probability distribution (Supplemental Tab. 2). The IPCC *Wetlands Supplement* Guidance reports methane and soil emissions factors using geometric means, which are similar to exponentiated logmeans as they approximate medians for some types of skewed distributions and that they decrease the influence of outliers. However arithmetic means of logmean distributed data are often more appropriate when scaling estimates up in space and time in order to estimate totals (Levy *et al* 2017). We performed a second version of uncertainty and sensitivity analyses using the mean of lognormally distributed data rather than the exponentiated logmean, to test the effect of this alternative assumption on uncertainty and sensitivity of total flux to inputs

3. Additional Results and Discussion

3.1. Estimated to Mapped Area Ratios

We would like to highlight a few interesting results from the Monte Carlo-based uncertainty estimates of C-CAP estimated to mapped area ratios (Supplemental Fig. 4). There is variation in both the scope and shape of errors. Within estuarine wetlands scrub/shrub wetland accuracy is overall lower than both emergent and forested wetlands. Estuarine forested wetlands have an asymmetric error distribution because the have relatively few validation samples (21) and exhibit only commission error. Palustrine emergent and scrub/shrub wetlands were under-mapped while, estuarine scrub/shrub, forested, and emergent were generally over-mapped. Of the key classes that conversion to and from led to the greatest uncertainty in our sensitivity analysis, estuarine aquatic beds, and unconsolidated shore showed a relatively great degree of uncertainty. Estuarine aquatic bed estimated to mapped area ratios Monte Carlo results exhibited a complex distribution; the majority of omission errors for this class were open water misclassified as estuarine aquatic bed. Because open water has a much larger area this effect is magnified when calculating uncertainty from a proportional area matrix.

Similarly, from 2006 to 2011 ‘no change’ was more uncertain as a class than ‘change’. In addition change is under-mapped as a category. This is different conclusion than the official C-CAP accuracy assessment drew (McCombs *et al* 2016). However, McCombs et al., calculated accuracy assessments using raw count rather than a proportional area matrix. Because no-change classes made up a much larger area, for change classes omission errors (errors of exclusion) ended up having a much greater proportional effect than commission errors (errors of inclusion). Thus, the differences between these two approaches.

3.2. How should we scale up positively skewed emissions factors: logmeans or means?

During the course of revising this manuscript we realized that for positively skewed emissions factors -- which we describe throughout using exponentiated lognormal distributions -- an argument could be made that we should be using mean values to scale up estimates of flux to the national level, rather than using exponentiated logmeans, which approximate medians for these types of distributions.

Simply put, median values are more appropriate for estimating how much CO_2e any individual point or site emits or buries, but a mean is more appropriate when scaling up and estimating the entire sum total of emissions and burials at a continental scale. While this followed logically we could not find any explicit guidance in the IPCC *Wetlands Supplement* or *Uncertainty* Chapters which we reference throughout the text. In fact almost all emissions factors in the *Wetlands Supplement* report geometric means, which are very similar to the logmeans we describe throughout, implying that we should scale up emissions factors while depressing the effects of positive outliers. Because the goal of this paper was to test the effects of assumptions, dataset uncertainty, etc. on the overall accounting, we re-ran the Monte Carlo and sensitivity analyses replacing logmeans with means for summarising emissions factors from lognormally distributed variables (soil carbon burial rates, palustrine methane emissions, and forested, scrub/shrub, and emergent biomass).

Simulated total flux values when using only means as emissions factors were more extreme and far more uncertain than when using logmeans (Supplemental Fig. 4). The sum total of the accounting as far more uncertain than previously with a long tail going into the extreme net-emissions. Palustrine CH_4 emissions in particular introduced far more uncertainty when using means (Supplemental Fig. 5). Palustrine methane emissions introduced 79.3 million tonnes of CO_2e per year of uncertainty into the overall accounting. The upper 95% CI on a simulated mean palustrine methane emissions using GWP for converting to CO_2e (643 to 6849 gCO_2e m^{-2} yr^{-1}) was greater than the maximum value of the dataset (5333 gCO_2e m^{-2} yr^{-1}). The top contributors to uncertainty ranked by the sensitivity analysis shifted when relying on means with other inputs that affect the net flux of palustrine methane emissions gaining more uncertainty (the method for mapping palustrine coastal wetlands [NWI vs Coastal Lands], and the conversion factor used to estimate CO_2e from CH_4 [GWP vs SGW/CP]).

These results could be interpreted in two ways ways. First we originally thought this could be an indication that the Monte Carlo simulation technique we were using had the potential itself to introduce unreasonably high values. However we estimated the CI of using an Cox Method approximation (Eq. 10-11) (Olsson 2005) and found the two estimates to agree in terms of scale (691 to 7318 gCO_2e m^{-2} yr^{-1}). Future iterations of these uncertainty simulations could rely on a bootstrapping approach to estimate CIs, which would effectively constrain CI's by the upper and lower limits of the observed dataset. This could be reasonable if there were a process-based justification for assuming an upper limit on methane emissions, but it would also introduce a major assumption that would need to be justified.

$$\mu = exp(\alpha + 0.5\beta^2) \qquad 10.$$

$$CI \ = exp(\alpha + 0.5\beta^2) \ \pm 1.96\sqrt{\frac{\beta^2}{n} + \frac{\beta^4}{2(n-1)}}) \qquad 11.$$

In which:

mu = approximate arithmatic mean
alpha = mean of log transformed data
beta = standard deviation of the log transformed data
CI = confidence interval
n = number of datapoints

Second, the palustrine wetland methane emissions subset is very small, only 24 data points. This could be interpreted to mean that the high amount of uncertainty observed in this second iteration is very real, and we should consider the possibility of mean values being higher than observed given such a small dataset. Third and finally we need to consider whether these outliers in palustrine wetland methane emissions represent landscape-level variability in annual emissions, or are they the results of outliers caused by the temporal windows, the frequency of sampling, or the variety in methodology. This question, especially for methane emissions, is not new to this study (Krauss *et al* 2016), but is beyond the scope of our current effort.

Because there is not clear guidance on this issue, and extreme positively skewed uncertainty in methane emissions could either be caused by real landscape scale variability, or observational and methodological outliers, we ultimately decided that it would be the most conservative to leave our original analysis -- utilizing exponentiated logmeans to scale up lognormally distributed emissions factors -- as is; but we decided to include these observations and this discussion as supplemental information for the sake of transparency and to stimulate further discussion about the most appropriate methods to scale or coastal wetland GHG fluxes, and their inherent uncertainties, using the concepts of emissions factors and activities data.

Supplemental Table and Figures:

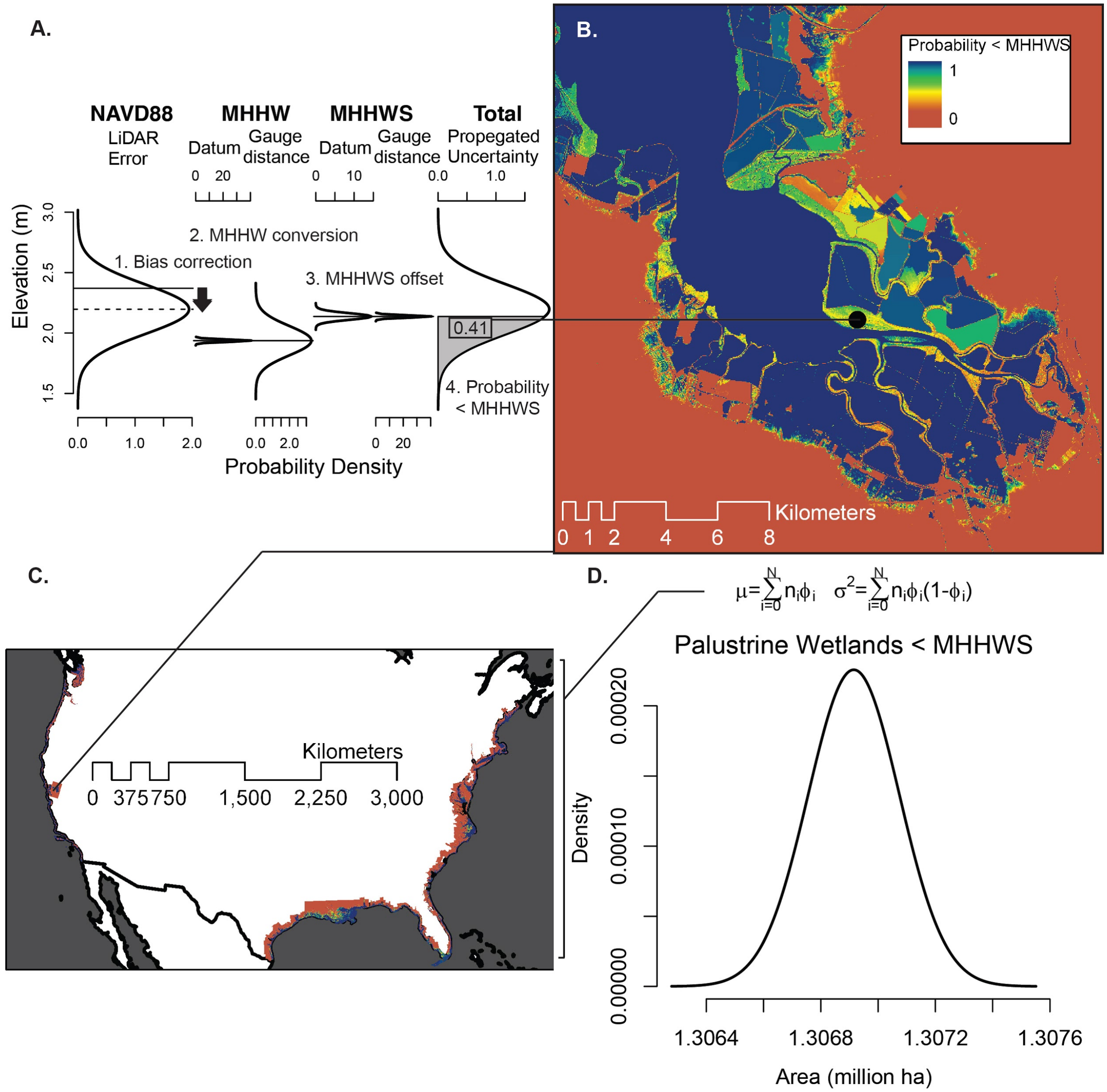

Supplemental Figure 1: A. Process for calculating probabilistic coastal lands layer (1.) correcting for mean LiDAR bias for wetland surfaces (2.) converting the orthometric height (NAVD88) to a tidal surface (mean higher high water [MHHW]), and (3) estimating mean higher high water spring (MHHWS) using a local offset. Each conversion has one or more sources of uncertainty associated it. We calculated propagated uncertainty and (4) probability of a pixel falling below MHHWS. B. Probabilistic MHHWS for South San Francisco Bay. C. CONUS-scale extent of this mapping. D. The probabilities of all these pixels were summarized at the national level, using a binomial normal approximation.

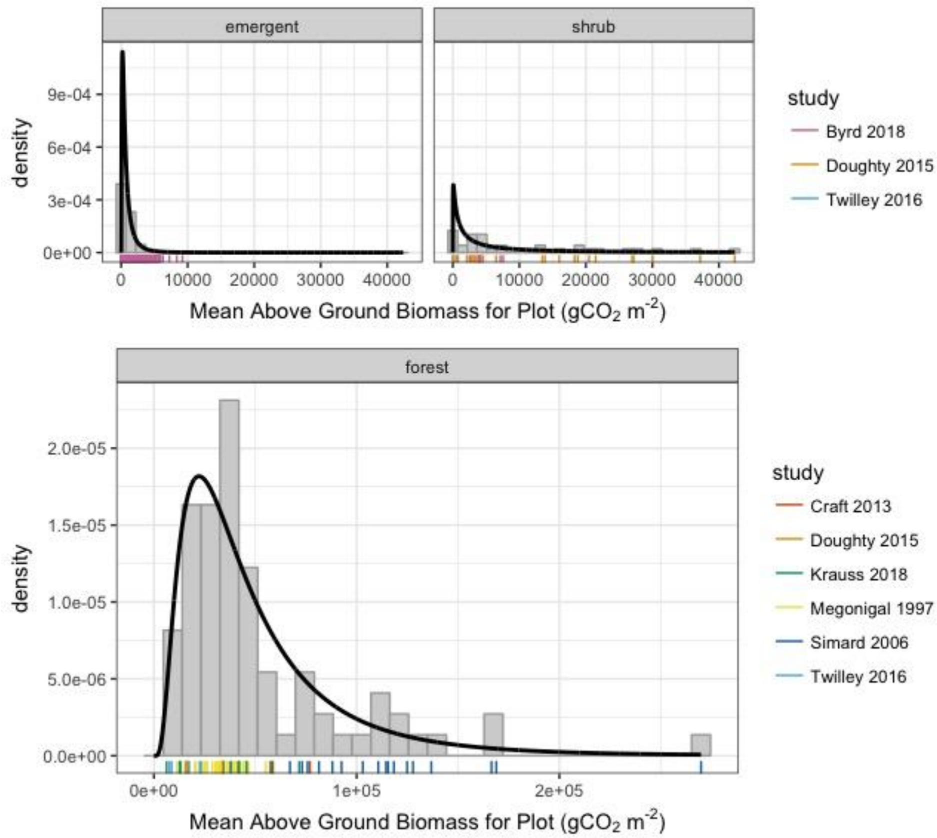

Supplemental Figure 2: Biomass stocks and probability distributions used in the Monte Carlo Analysis for emergent, scrub/shrub, and forested wetlands. Data sources are pictured by colored lines to emphasize inter-study system-specific variability.

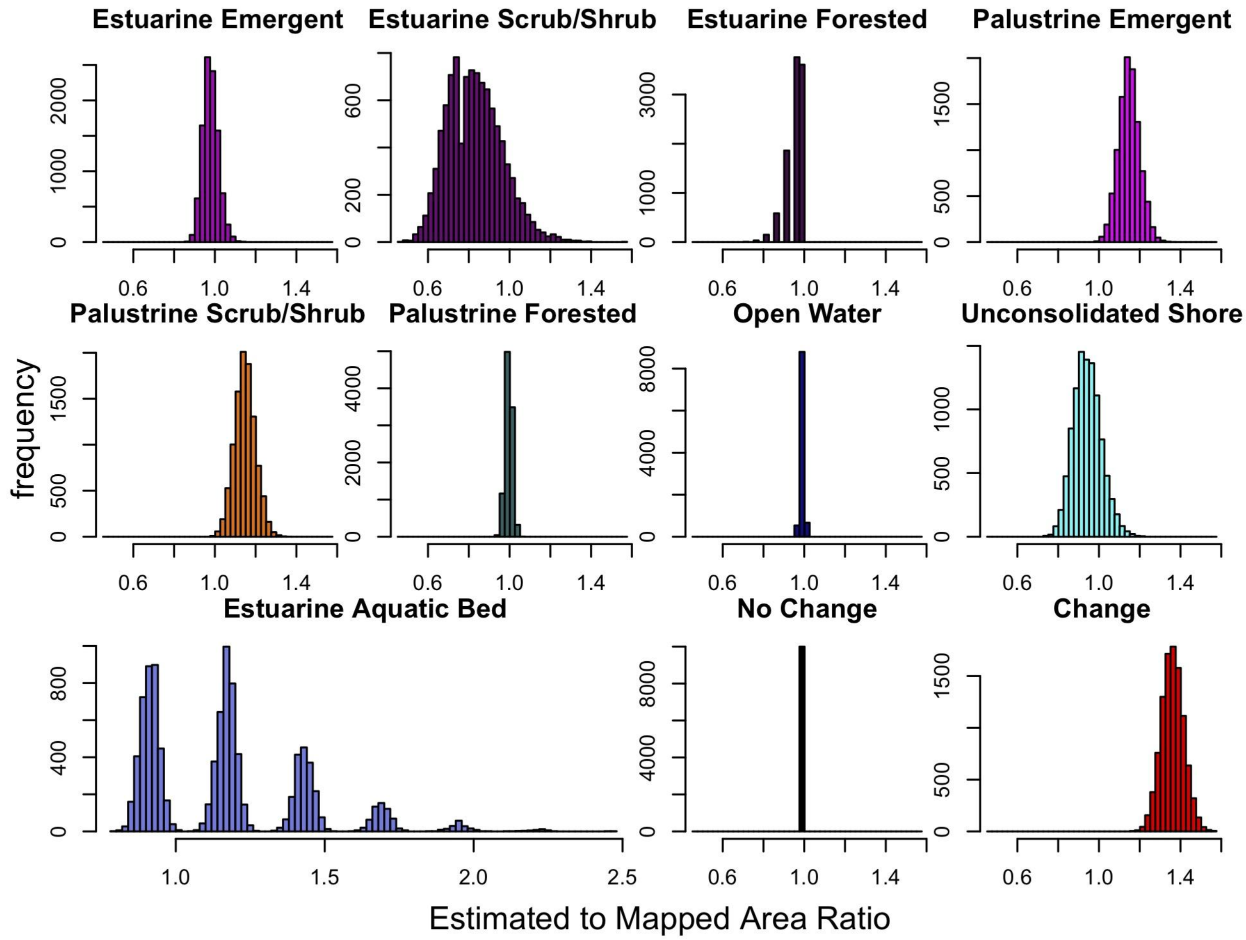

Supplemental Figure 3: Histograms show the result of the Monte Carlo uncertainty analysis for key C-CAP estimated to mapped area ratios. These include the six 2011 wetland classifications, and three common 2010 classifications that can represent erosion, counting as a catastrophic soil loss, as well as 2006 to 2011 change and no-change overall. Values great than 0 are under-mapped at the national scale. Values lower than 0 are over-mapped at the national scale.

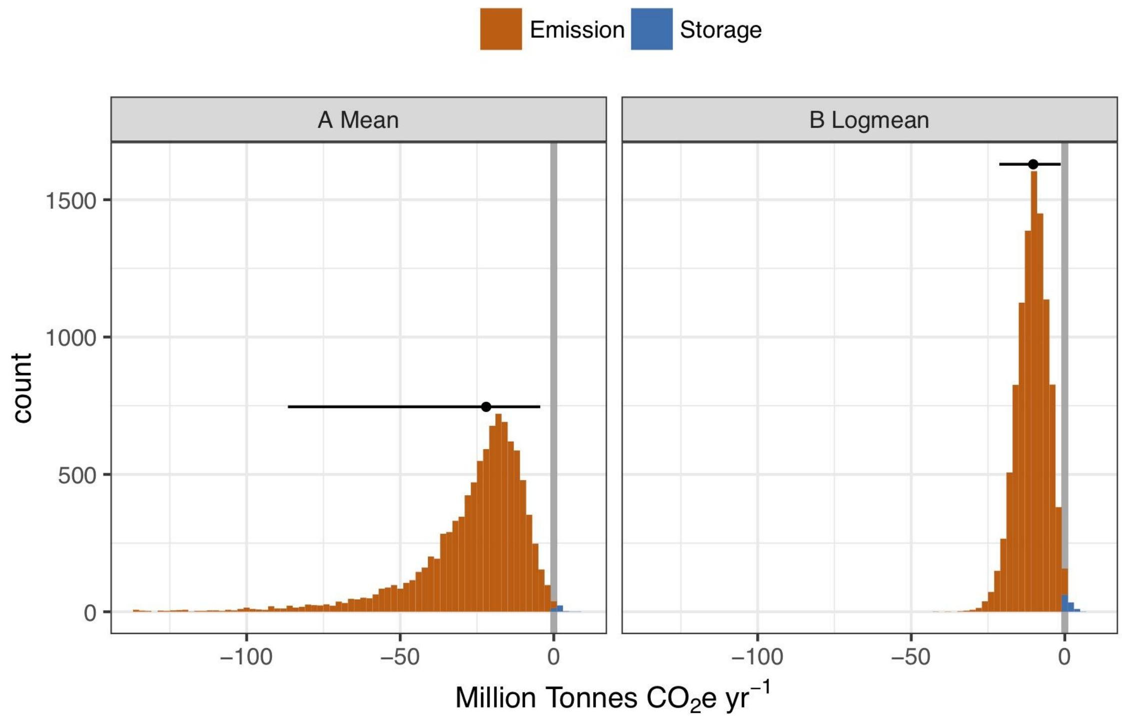

Supplemental Figure 4: Comparison of 10,000 different randomized iterations of the U.S. coastal national greenhouse gas inventory. Left: utilizing arithmetic means for lognormally distributed emissions factors. Right: utilizing exp(logmean) (similar to the median) for lognormally distributed emissions factors.

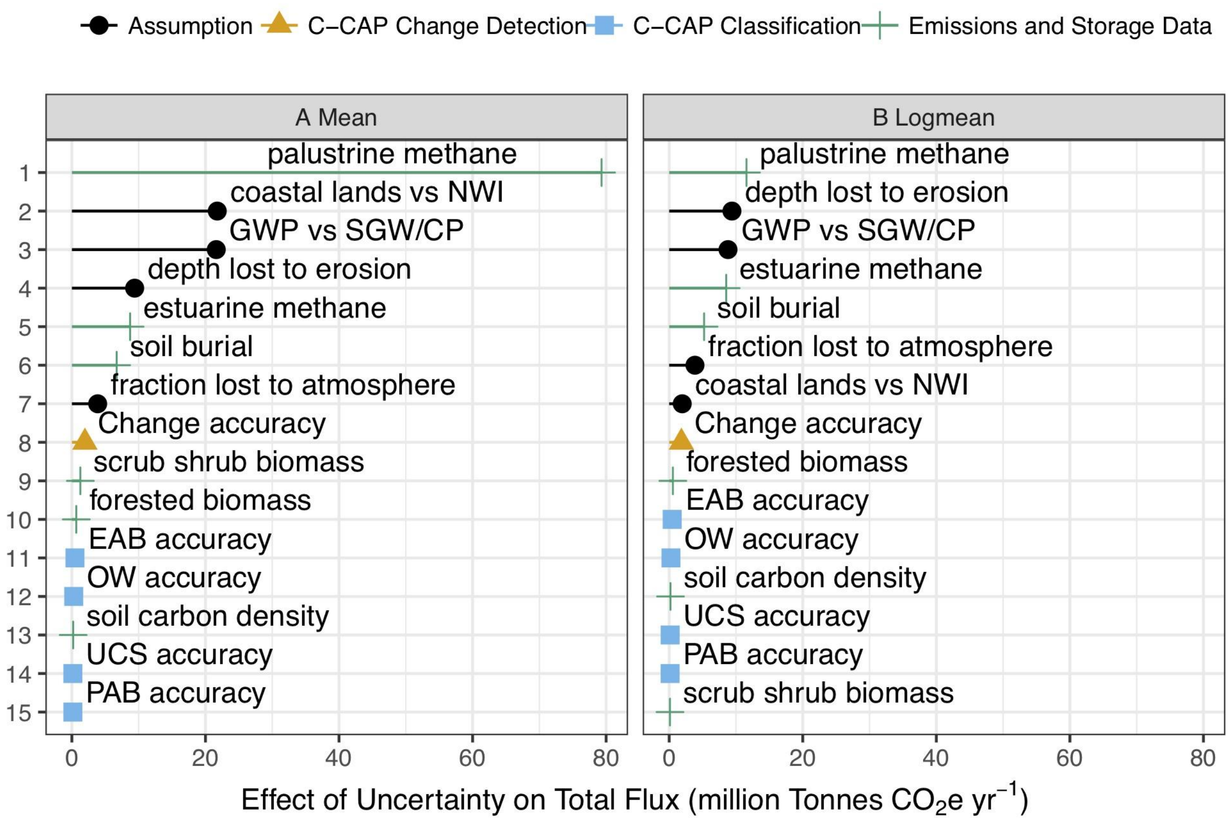

Supplemental Figure 5: Comparison of the top fifteen inputs introducing the most uncertainty into the Coastal Wetland National Greenhouse Gas Inventory (NGGI) according to one-at-a-time sensitivity analyses. Left: Strategy utilized arithmatic means for lognormally distributed emissions factors. Right: Utilized exp(logmean) (similar to the median) for lognormally distributed emissions factors. GWP: Global Warming Potential, SGWP: Sustained GWP, SGCP: Sustained Global Cooling Potential, NWI: National Wetlands Inventory, EAB: Estuarine Aquatic Bed, OW: Open Water, UCS: Unconsolidated Shore, PAB: Palustrine Aquatic Bed.

Supplemental Table 1: The names and sources of digital elevation models and land cover maps used in the analysis

Supplemental Table 2: The results of a literature review of four studies comparing real-time kinematic global positioning system elevation measurements to elevation models based on light detection and ranging. The bottom row shows how we calculated a weighted average mean error (ME) and root mean square error (RMSE) from the various studies and the number of datapoints (n).

Supplemental Table 3: Mapped pixel counts for each sub-class. Each pixel is 30 x 30 m. Estuarine wetlands are fixed values. Palustrine values are defined as a normal with a mean and standard deviation. These were estimated from binomial normal approximations from the probabilistic MHHWS mapping.

Supplemental Table 4: C-CAP 2011 Class Accuracy Assessment Data (McCombs *et al* 2016) with total 2011 C-CAP mapped areas used to calculate estimated area. Definition of abbreviations: HID = High Intensity Developed, MID = Medium Intensity Developed, LID = Low Intensity Developed, OSD = Developed Open Space, CULT = Cultivated, PAST = Pasture, GRS = Grassland, DEC = Deciduous Forest, EVR = Evergreen Forest, MIX = Mixed Forest, SS = Scrub/Shrub, PFW = Palustrine Forested Wetland, PSS = Palustrine Scrub/Shrub Wetland, PEM = Palustrine Emergent Wetland, EFW = Estuarine Forested Wetland, ESS = Estuarine Scrub/Shrub Wetland, EEM = Estuarine Emergent Wetland, UCS = Unconsolidated Shore, BAR = Bare Land, OW = Open Water, PAB = Palustrine Aquatic Bed, EAB = Estuarine Aquatic Bed, SNOW = Snow.

Supplemental Table 5: C-CAP 2006 to 2011 Change Detection Accuracy Assessment Data (McCombs *et al* 2016) with total 2006 to 2011 C-CAP mapped areas used to calculate estimated area.

Supplemental Table 6: The results of the entire Monte Carlo Uncertainty Analysis. These include the minimum (0.025 quantile), median (0.5 quantile) and maximum (0.975 quantile) distribution of total scenario results for each relevant mapped land cover type and land cover change type from 2006 to 2011 according to the coastal change analysis program. We also present the confidence interval range. We present the results of mapped area and estimated area as pixel counts, and total flux, soil flux, biomass flux, a methane flux as tonnes CO_2e per year per mapped pixel. Positive values indicate storage, negative values emissions.

Supplemental Table 7: Full results of the one-at-a-time sensitivity analysis. Each parameter is listed along with what type of contribution it makes to the inventory, and what effect it has on the inventory total in tonnes CO_2e per year.

References:

Bartlett K B, Bartlett D S, Harriss R C and Sebacher D I 1987 Methane emissions along a salt marsh salinity gradient *Biogeochemistry* **4** 183–202

Bartlett K B, Harriss R C and Sebacher D I 1985 Methane flux from coastal salt marshes *J. Geophys. Res.* **90** 5710–20

Bianchi T S, Allison M A, Zhao J, Li X, Comeaux R S, Feagin R A and Kulawardhana R W 2013 Historical reconstruction of mangrove expansion in the Gulf of Mexico: Linking climate change with carbon sequestration in coastal wetlands *Estuar. Coast. Shelf Sci.* **119** 7–16

Buffington K J, Dugger B D, Thorne K M and Takekawa J Y 2016 Statistical correction of lidar-derived digital elevation models with multispectral airborne imagery in tidal marshes *Remote Sens. Environ.* **186** 616–25

Byrd K B, Ballanti L, Thomas N, Nguyen D, Holmquist J R, Simard M and Windham-Myers L 2018 A remote sensing-based model of tidal marsh aboveground carbon stocks for the conterminous United States *ISPRS J. Photogramm. Remote Sens.* **139** 255–71

Callaway J C, Borgnis E L, Eugene Turner R and Milan C S 2012a Carbon Sequestration and Sediment Accretion in San Francisco Bay Tidal Wetlands *Estuaries Coasts* **35** 1163–81

Callaway J C, Borgnis E L, Turner R E, Milan C S, Goodfriend W and Richmond S 2012b *Wetland Sediment Accumulation at Corte Madera Marsh and Muzzi Marsh* Online: https://pdfs.semanticscholar.org/83c3/6e773f9a54d6dee346147ba742e8afd167a9.pdf

Chmura G L, Kellman L, van Ardenne L and Guntenspergen G R 2016 Greenhouse Gas Fluxes from Salt Marshes Exposed to Chronic Nutrient Enrichment *PLoS One* **11** e0149937

Church T M, Sommerfield C K, Velinsky D J, Point D, Benoit C, Amouroux D, Plaa D and Donard O F X 2006 Marsh sediments as records of sedimentation, eutrophication and metal pollution in the urban Delaware Estuary *Mar. Chem.* **102** 72–95

Continuum Analytics, Inc 2017 *Python*

Craft C B and Richardson C J 1998 Recent and Long-Term Organic Soil Accretion and Nutrient Accumulation in the Everglades *Soil Sci. Soc. Am. J.* **62** 834–43

Craft C B, Stahl M, Widney S and Smith D 2017 Forest survey of species richness and basal area for two tidal forest plots at GCE 11 on the Altamaha River in Southeast Georgia in December 2013 Online: http://dx.doi.org/10.6073/pasta/95771dba9e839a57c74b9ae806569877

Crooks S, Rybczyk J, O’Connell K, Devier D L, Poppe K and Emmett-Mattox S 2014 Coastal blue carbon opportunity assessment for the Snohomish Estuary: The climate benefits of estuary restoration *Report by Environmental Science Associates, Western Washington University, EarthCorps, and Restore America’s Estuaries*

DeLaune R D, Smith C J and Patrick W H 1983 Methane release from Gulf coast wetlands *Tellus B Chem. Phys. Meteorol.* **35B** 8–15

Doughty C L, Adam Langley J, Walker W S, Feller I C, Schaub R and Chapman S K 2016

Mangrove Range Expansion Rapidly Increases Coastal Wetland Carbon Storage *Estuaries Coasts* **39** 385–96

Eastern Shore Regional GIS Cooperative Maryland iMAP Pre-Defined DEMs Online: http://imap.maryland.gov/Pages/lidar-dem-download-files.aspx

Esri Inc. 2017 *ArcGIS Pro*

Hladik C, Schalles J and Alber M 2013 Salt marsh elevation and habitat mapping using hyperspectral and LIDAR data *Remote Sens. Environ.* **139** 318–30

Holm G O, Perez B C, McWhorter D E, Krauss K W, Johnson D J, Raynie R C and Killebrew C J 2016 Ecosystem Level Methane Fluxes from Tidal Freshwater and Brackish Marshes of the Mississippi River Delta: Implications for Coastal Wetland Carbon Projects *Wetlands* **36** 401–13

Holmquist J R, Megonigal P and Lynch J in Prep Global Change Research Wetland 2016 Elevation Survey Data

Holmquist J R, Windham-Myers L, Bliss N, Crooks S, Morris J T, Megonigal J P, Troxler T, Weller D, Callaway J, Drexler J, Ferner M C, Gonneea M E, Kroeger K D, Schile-Beers L, Woo I, Buffington K, Breithaupt J, Boyd B M, Brown L N, Dix N, Hice L, Horton B P, MacDonald G M, Moyer R P, Reay W, Shaw T, Smith E, Smoak J M, Sommerfield C, Thorne K, Velinsky D, Watson E, Grimes K W and Woodrey M 2018 Accuracy and Precision of Tidal Wetland Soil Carbon Mapping in the Conterminous United States *Sci. Rep.* **8** 9478

Hussein A H, Rabenhorst M C and Tucker M L 2004 Modeling of carbon sequestration in coastal marsh soils *Soil Sci. Soc. Am. J.* **68** 1786

IPCC 2014 *2013 Supplement to the 2006 IPCC Guidelines for National Greenhouse Gas Inventories: Wetlands* ed T Hiraishi, T Krug, K Tanabe, N Srivastava, J Baasansuren, M Fukuda and T G Troxler (Switzerland: IPCC)

Iversen P, Lee D and Rocha M 2014 Understanding land use in the UNFCCC *Climate and Land Use Alliance*

Jenkins J C, Chojnacky D C, Heath L S and Birdsey R A 2003 National-Scale Biomass Estimators for United States Tree Species *For. Sci.* **49** 12–35

Kearney M S and Stevenson J C 1991 Island Land Loss and Marsh Vertical Accretion Rate Evidence for Historical Sea-Level Changes in Chesapeake Bay *J. Coast. Res.* **7** 403–15

Kelley C A, Martens C S and Ussler W 1995 Methane dynamics across a tidally flooded riverbank margin *Limnol. Oceanogr.* **40** 1112–29

Krauss K W, Holm G O, Perez B C, McWhorter D E, Cormier N, Moss R F, Johnson D J, Neubauer S C and Raynie R C 2016 Component greenhouse gas fluxes and radiative balance from two deltaic marshes in Louisiana: Pairing chamber techniques and eddy covariance *J. Geophys. Res. Biogeosci.* **121** 2015JG003224

Krauss K W, Noe G B, Duberstein J A, Conner W H, Jones M C, Bernhardt C E, Cormier N and From A S 2018 Carbon budget assessment of tidal freshwater forested wetland and oligohaline marsh ecosystems along the Waccamaw and Savannah rivers, U.S.A. (2005-2016) Online: http://dx.doi.org/10.5066/F7TM7930

Krauss K W and Whitbeck J L 2012 Soil Greenhouse Gas Fluxes during Wetland Forest Retreat along the Lower Savannah River, Georgia (USA) *Wetlands* **32** 73–81

Krivoruchko K 2012 Empirical bayesian kriging *Esri: Redlands, CA, USA* Online: http://www.esri.com/NEWS/ARCUSER/1012/files/ebk.pdf

Levy P E, Cowan N, van Oijen M, Famulari D, Drewer J and Skiba U 2017 Estimation of cumulative fluxes of nitrous oxide: uncertainty in temporal upscaling and emission factors *Eur. J. Soil Sci.* **68** 400–11

Lu M, Bernal B, Holmquist J R and Megonigal J P 2017 *Coastal-Wetland-NGGI-Data-Public* (Github) Online: https://github.com/Smithsonian/Coastal-Wetland-NGGI-Data-Public

Lynch J C 1989 *Sedimentation and nutrient accumulation in mangrove ecosystems of the Gulf of Mexico* (University of Southwestern Louisiana)

Magenheimer J F, Moore T R, Chmura G L and Daoust R J 1996 Methane and carbon dioxide flux from a macrotidal salt marsh, Bay of Fundy, New Brunswick *Estuaries* **19** 139–45

Marchio D A, Savarese M, Bovard B and Mitsch W J 2016 Carbon Sequestration and Sedimentation in Mangrove Swamps Influenced by Hydrogeomorphic Conditions and Urbanization in Southwest Florida *For. Trees Livelihoods* **7** 116

Marsh A S, Rasse D P, Drake B G and Patrick Megonigal J 2005 Effect of elevated CO2 on carbon pools and fluxes in a brackish marsh *Estuaries* **28** 694–704

McCombs J W, Herold N D, Burkhalter S G and Robinson C J 2016 Accuracy Assessment of NOAA Coastal Change Analysis Program 2006-2010 Land Cover and Land Cover Change Data *Photogrammetric Engineering & Remote Sensing* **82** 711–8

Medeiros S, Hagen S, Weishampel J and Angelo J 2015 Adjusting Lidar-Derived Digital Terrain Models in Coastal Marshes Based on Estimated Aboveground Biomass Density *Remote Sensing* **7** 3507–25

Megonigal J P, Conner W H, Kroeger S and Sharitz R R 1997 ABOVEGROUND PRODUCTION IN SOUTHEASTERN FLOODPLAIN FORESTS: A TEST OF THE SUBSIDY–STRESS HYPOTHESIS *Ecology* **78** 370–84

Megonigal J P, Schlesinger W and Others 2002 Methane-limited methanotrophy in tidal freshwater swamps *Global Biogeochem. Cycles* **16** Online: http://onlinelibrary.wiley.com/doi/10.1029/2001GB001594/full

Merrill J Z 1999 *Tidal Freshwater Marshes as Nutrient Sinks: particulate Nutrient Burial and Denitrification* (University of Maryland, College Park)

Mersmann O, Trautmann H, Steuer D and Bornkamp B 2018 truncnorm: Truncated Normal Distribution Online: https://CRAN.R-project.org/package=truncnorm

Microsoft Corporation and Weston S 2017 doSNOW: Foreach Parallel Adaptor for the “snow” Package Online: https://CRAN.R-project.org/package=doSNOW

Microsoft and Weston S 2017 foreach: Provides Foreach Looping Construct for R Online: https://R-Forge.R-project.org/projects/foreach/

Mueller P, Hager R N, Meschter J E, Mozdzer T J, Adam Langley J, Jensen K and Patrick Megonigal J 2016 Complex invader-ecosystem interactions and seasonality mediate the impact of non-native Phragmites on CH4 emissions *Biol. Invasions* **18** 2635–47

Neubauer S C 2013 Ecosystem Responses of a Tidal Freshwater Marsh Experiencing Saltwater Intrusion and Altered Hydrology *Estuaries Coasts* **36** 491–507

Neubauer S C, Miller W D and Anderson I C 2000 Carbon cycling in a tidal freshwater marsh ecosystem: a carbon gas flux study *Mar. Ecol. Prog. Ser.* **199** 13–30

NOAA 2013 C-CAP 2006-2010-Era Land Cover Change Data Online: https://coast.noaa.gov/ccapftp/

NOAA 2017 Datums Online: https://tidesandcurrents.noaa.gov/stations.html?type=Datums

NOAA Datums Error East Coast Online: https://tidesandcurrents.noaa.gov/pdf/Datums_error_east_coast.pdf

NOAA Datums Error Gulf Coast Online: https://tidesandcurrents.noaa.gov/pdf/Datums_error_gulf_coast.pdf

NOAA Datums Error West Coast Online: https://tidesandcurrents.noaa.gov/pdf/Datums_error_west_coast.pdf

NOAA 2016 Sea-level rise data download: DEM Online: https://coast.noaa.gov/slrdata/

NOAA CO-OPS Water Level Data, Verified, High Low Online: https://data.noaa.gov/dataset/nos-co-ops-water-level-data-verified-high-low

NOAA Office of Coastal Management *Coastal Change Analysis Program (C-CAP) Land Cover Classifications* Online: https://coast.noaa.gov/data/digitalcoast/pdf/ccap-class-scheme-regional.pdf

Noe G B, Hupp C R, Bernhardt C E and Krauss K W 2016 Contemporary Deposition and Long-Term Accumulation of Sediment and Nutrients by Tidal Freshwater Forested Wetlands Impacted by Sea Level Rise *Estuaries Coasts* **39** 1006–19

NumPy Developers 2017 *NumPy* Online: http://www.numpy.org/l

Olofsson P, Foody G M, Herold M, Stehman S V, Woodcock C E and Wulder M A 2014 Good practices for estimating area and assessing accuracy of land change *Remote Sens. Environ.* **148** 42–57

Olsson U 2005 Confidence Intervals for the Mean of a Log-Normal Distribution *J. Stat. Educ.* **13** null – null

Orson R A, Warren R S and Niering W A 1998 Interpreting Sea Level Rise and Rates of Vertical Marsh Accretion in a Southern New England Tidal Salt Marsh *Estuar. Coast. Shelf Sci.* **47** 419–29

Pilz J and Spöck G 2008 Why do we need and how should we implement Bayesian kriging methods *Stoch. Environ. Res. Risk Assess.* **22** 621–32

Poffenbarger H J, Needelman B A and Megonigal J P 2011 Salinity Influence on Methane Emissions from Tidal Marshes *Wetlands* **31** 831–42

R Core Team 2017 R: A Language and Environment for Statistical Computing Online: https://www.R-project.org/

Reid M C, Tripathee R, Schäfer K V R and Jaffé P R 2013 Tidal marsh methane dynamics: Difference in seasonal lags in emissions driven by storage in vegetated versus unvegetated sediments *J. Geophys. Res. Biogeosci.* **118** 1802–13

Revolution Analytics and Weston S 2015 doParallel: Foreach Parallel Adaptor for the “parallel” Package Online: https://R-Forge.R-project.org/projects/doparallel/

Roman C T, Peck J A, Allen J R, King J W and Appleby P G 1997 Accretion of a New England (USA) salt marsh in response to inlet migration, storms, and sea-level rise *Estuar. Coast. Shelf Sci.* **45** 717–27

Schmid K, Hadley B and Waters K 2013 Mapping and Portraying Inundation Uncertainty of Bathtub-Type Models *J. Coast. Res.* 548–61

Segarra K E A, Comerford C, Slaughter J and Joye S B 2013 Impact of electron acceptor availability on the anaerobic oxidation of methane in coastal freshwater and brackish wetland sediments *Geochim. Cosmochim. Acta* **115** 15–30

Simard M, Zhang K, Rivera-Monroy V H, Ross M S, Ruiz P L, Castañeda-Moya E, Twilley R R and Rodriguez E 2006 Mapping Height and Biomass of Mangrove Forests in Everglades National Park with SRTM Elevation Data *Photogrammetric Engineering & Remote Sensing* **72** 299–311

Smith T J and Whelan K R T 2006 Development of allometric relations for three mangrove species in South Florida for use in the Greater Everglades Ecosystem restoration *Wetlands Ecol. Manage.* **14** 409–19

Sonderegger D 2012 *SiZer: Significant Zero Crossings* Online: http://www.r-project.org

Twilley R, Rivera-Monroy V and Castaneda E 2018 Mangrove Forest Growth from the Shark River Slough, Everglades National Park (FCE), South Florida from January 1995 to Present Online: http://dx.doi.org/10.6073/pasta/0c8f485c7095dfed160e66b9b959f470

USGS 2014 Topobathymetric Elevation Model of Northern Gulf of Mexico Online: https://topotools.cr.usgs.gov/coned/ngom.php

USNO Phases of the Moon Online: http://aa.usno.navy.mil/data/docs/MoonPhase.php

Villa J A and Mitsch W J 2015 Carbon sequestration in different wetland plant communities in the Big Cypress Swamp region of southwest Florida *Int. J. Biodivers. Sci. Eco. Srvcs. Mgmt.* **11** 17–28

Wang R-F and Ateljevich E 2012 San Francisco Bay and Sacramento-San Joaquin Delta DEM *Methodology for Flow and Salinity Estimates in the Sacramento-San Joaquin Delta and*

Suisun Mars, 23rd Annual Progress Report to the State Water Resources Control Board Online: http://baydeltaoffice.water.ca.gov/modeling/deltamodeling/modelingdata/DEM.cfm

Weston N B, Neubauer S C, Velinsky D J and Vile M A 2014 Net ecosystem carbon exchange and the greenhouse gas balance of tidal marshes along an estuarine salinity gradient *Biogeochemistry* **120** 163–89

Wilson B J, Mortazavi B and Kiene R P 2015 Spatial and temporal variability in carbon dioxide and methane exchange at three coastal marshes along a salinity gradient in a northern Gulf of Mexico estuary *Biogeochemistry* **123** 329–47

Windham-Myers L and Cai W-J in Revision Chapter 15. Tidal Wetlands and Estuaries *SOCCR-2 Fourth Order Draft*